Available online at www.sciencedirect.com
ScienceDirect
Journal of Catalysis 252 (2007) 231–242
JOURNAL OF CATALYSIS
www.elsevier.com/locate/jcat

The role of cationic Au^{3+} and nonionic Au^0 species in the low-temperature water–gas shift reaction on Au/CeO_2 catalysts

A. Karpenko [a], R. Leppelt [a], V. Plzak [b], R.J. Behm [a,*]

[a] *Institute of Surface Chemistry and Catalysis, Ulm University, D-89069 Ulm, Germany*
[b] *Center of Solar Energy and Hydrogen Research, Helmholtzstr. 8, D-89081 Ulm, Germany*

Received 22 August 2007; revised 24 September 2007; accepted 24 September 2007

Available online 29 October 2007

Abstract

The roles of cationic and nonionic Au species in the water–gas shift (WGS) reaction on Au/CeO_2 catalysts were studied by comparing the reaction behavior of a cyanide leached catalyst, after removal of the Au nanoparticles by cyanide leaching, with that of non-leached catalysts, following the technique introduced by Q. Fu et al. [Science 301 (2003) 935]. Using rate measurements as well as in situ spectroscopic and structure-sensitive techniques, we found that based on the Au mass balance, cyanide leaching removed all Au except for ionic Au^{3+} species, and that leaching resulted in a pronounced decay of the catalyst mass normalized activity to 1–25% of that of a non-leached catalyst. The extent of the activity loss strongly depended on the post-treatment of the leached catalyst. Both the catalyst treatment after leaching and, in particular, the WGS reaction resulted in considerable reformation of Au^0 species by thermal decomposition of Au oxides (Au^{3+}) and subsequent nucleation and growth of very small Au^0 aggregates and metallic Au^0 nanoparticles, as indicated by Au(4f) signals at 85.9 eV (Au^{3+}), 84.0–84.6 eV (up-shifted signal of small Au^0 aggregates), and 84.0 eV (metallic Au^0). In this work, correlations between ionic and nonionic Au species and between total WGS activity and activity for the formation/decomposition of bidentate formate species are evaluated, and the role of the respective Au species in the WGS reaction on Au/CeO_2 catalysts is discussed.

Keywords: Water–gas shift reaction; Au catalyst; Active center; Activity; Deactivation; Au/CeO_2

1. Introduction

Au/CeO_2 catalysts have been reported to be highly active catalysts for the water–gas shift (WGS) reaction (see [1] and references therein). Despite numerous studies, the exact origin of the high reactivity and the underlying reaction mechanism remain under debate. The present study focused on two different aspects: identification of the active center and the reaction intermediates in the rate-limiting step, and description of the overall reaction mechanism, including the different reaction steps and possibly different reaction pathways.

The question of the active sites for CO removal in the WGS reaction is controversial. The activity is clearly related to the presence of Au, either as nanoparticles or as ionic species, because under these conditions, the activity of pure ceria is orders of magnitude lower than that of Au/CeO_2 catalysts [2–5]. Based on elegant leaching experiment, in which Au nanoparticles were removed from the catalyst by cyanide leaching and the activity before and after leaching was compared, Fu et al. [6–9] proposed ionic Au^{n+} species to represent the active center in the WGS reaction, with Au^0 acting as spectator only. In contrast to this proposal are the findings of Kim and Thompson [10], who observed a significant reduction in WGS activity on Au leaching when applying the same kind of leaching procedure and thus concluded that nanocrystalline gold represents the active site for the WGS reaction. For reaction at higher temperatures (above 250 °C), small Au^0 clusters and O vacancy sites on ceria were claimed to be the active centers of Au/CeO_2 catalysts for the WGS reaction [11]. Cationic gold was considered unstable under these conditions and thus was excluded as an active center. Burch et al. [1] proposed small metallic gold clusters in intimate contact with the oxide support as the active centers

* Corresponding author.
E-mail address: juergen.behm@uni-ulm.de (R.J. Behm).

0021-9517/$ – see front matter
doi:10.1016/j.jcat.2007.09.017

in the WGS reaction based on X-ray absorption measurements and density function theory (DFT) calculations [12], with the latter showing that a single Au atom is more strongly adsorbed on a Ce substitutional site in a CeO_2 surface than in an O substitutional site or on top of the surface, and that these Ce substitutional Au atoms are positively charged. On the other hand, our investigation of the effect of different pretreatment procedures on WGS activity demonstrated no clear correlation between the activity and the content of Au^{3+} or Ce^{3+} species [13]. The ceria surface is generally considered to provide formate and carbonate storage [5,14–18], to enable dissociation of water to OH_{ad} groups [15,19–21], and to stabilize metal particles [15,22–24].

The question of the reactive intermediate—more precisely, of the reactive intermediate in the dominant reaction pathway rate—also is under debate. Based on the appearance of formate bands, Tabakova et al. [20] suggested that formate species act as reaction intermediates on a Au/CeO_2 catalyst produced by the reaction of CO adsorbed on $Au^{\delta-}$ and OH groups located on Ce^{3+} [20]. Our group previously proposed a rather similar mechanism, but through an adsorbed formate intermediate, for the dominant reaction pathway [5,14]. This proposal was substantiated by a quantitative evaluation of the formate decomposition rate under reaction conditions, which was found to be of similar magnitude as the WGS rate under those conditions [5]. The rate-limiting character of formate decomposition is also demonstrated by the pronounced accumulation of adsorbed formate on the ceria surface. On the other hand, Meunier and coworkers suggested that carbonate species act as intermediate species, with formate acting as a byproduct, for the RWGS [25–27] and WGS [28,29] reaction on (La doped) Au/CeO_2 [28,29] and Pt/CeO_2 [25–27] catalysts. It is likely that different reaction pathways exist for these reactions [5,29], however, and that depending on the reaction conditions, reaction atmosphere, and catalyst pretreatment, the dominant reaction pathway, and hence the reaction intermediate, may change [1].

Overall, the situation remains controversial. The proposed role of the active sites was based mostly on indirect evidence, and the leaching experiments (which can be considered the most direct approach to determining the active site) led to divergent results. Furthermore, it is likely that the dominant reaction pathway for the WGS reaction on Au/CeO_2 catalysts depends on the reaction conditions, which also would result in different active sites for different reaction conditions [1,15].

In this work, we report results of a more extensive study on the activity and deactivation behavior of leached Au/CeO_2 catalyst, comparing the reaction behavior of two different types of catalysts, which should differ distinctly in the chemical state of the remaining Au species. In the type of catalyst vacuum-dried after leaching, the remaining Au should be present as ionic Au^{n+} species. For the other type, which was calcined at 400 °C after leaching, we expect that part of the ionic Au species is reconverted into Au^0 nanoparticles. After leaching, the remaining Au content was evaluated by inductively coupled plasma atom emission spectroscopy (ICP-AES). The particle size and the catalyst surface composition were determined by transmission electron microscopy (TEM) and X-ray photoemission spectroscopy (XPS). The activity and deactivation of the catalysts during the WGS reaction in dilute water gas (1 kPa CO, 2 kPa H_2O in N_2) were investigated in kinetic and spectroscopic measurements, including in situ IR measurements in a diffuse reflectance infrared Fourier transform spectroscopy (DRIFTS) configuration.

2. Experimental

2.1. Catalyst preparation

The catalysts were prepared by a deposition–precipitation procedure, using commercial CeO_2 as support (HSA 15, from Rhodia) and $HAuCl_4 \cdot 4H_2O$ for the deposition of Au. Further details are given in Refs. [30,31]. For removal of the Au nanoparticles, we used the same leaching procedure as described previously [6,8,9], but applying it to an unconditioned raw catalyst rather than to a calcined catalyst as in those previous studies. The initial and remaining Au metal contents were determined by ICP-AES. All measurements were carried out using catalysts with ca. 2.7 wt% (78 $m^2\,g^{-1}$) and 2.8 wt% (188 $m^2\,g^{-1}$) Au loading. Conditioning of the raw catalysts was performed by first heating them in a N_2 stream to 200 °C, then keeping them at this temperature for 30 min, and finally treating them in a reductive atmosphere (10% H_2/N_2, *H200*) for 45 min. Subsequently, they were kept for another 30 min at the conditioning temperature in an N_2 stream, and then cooled to the reaction temperature in N_2 [13]. The leached catalysts were treated either by drying in vacuum (overnight at room temperature, *L025*) or by vacuum drying and subsequent calcination in air (for 2 h at 400 °C, *LC400*). After calcination, the catalysts were cooled in air. Before the WGS measurements, all catalysts except those pretreated in H_2 were heated in N_2 to 200 °C and kept at this temperature for 90 min. Then they were cooled in N_2 to reaction temperature, after which the gas was changed to the reaction gas mixture.

2.2. Catalyst characterization

The chemical composition of the catalysts was characterized by XPS (PHI 5800 ESCA), using monochromatized AlK_α radiation. Survey spectra were measured at binding energies (BEs) of 0–1400 eV. Detail spectra of the Au(4f) region were recorded in the range of 75–100 eV (0.125 eV and 20 ms per step). To remove surface-charging effects, the BEs were calibrated using the $Ce^{4+}(3d^{10}4f^0V^n)$ (u''') signal at 916.6 eV as a reference [5,32]. XPS peak fitting was performed using a public XPS peak fit program (XPSPEAK4.1 by R. Kwok). The Au peaks were fitted by assuming three peaks at 84.0, 84.6, and 85.9 eV (see Section 3.1). The complex fitting of the Ce(3d) peaks followed a procedure described earlier [5,13]. For XPS measurements, catalyst conditioning was performed ex situ. TEM images were obtained on a CM20 (Phillips) electron microscope, operated at 200 kV (point-to-point resolution, 0.24 nm).

2.3. Activity measurements

The activity measurements were performed in a quartz tube microreactor (4 mm i.d., typically 75 mg of catalyst powder)

placed into a ceramic tube oven. To obtain differential conversions, the catalyst samples were diluted with α-Al_2O_3, which is not active for the reaction in the temperature range of this study (reaction temperature 180 °C). Dilute water gas (1 kPa CO, balance N_2 [dry] + 2 kPa H_2O, 180 °C, 60 Nml min^{-1}) was used as a reaction mixture. Water was added to the gas stream in a saturation unit. The influent and effluent gases were analyzed by online gas chromatography (DANI, GC 86.10) with H_2 as a carrier gas. High-purity gases from Westphalen (CO 4.7, N_2 6.0) were used without further purification. Mass and heat transport problems were negligible, with rates $<10^{-5}$ mol s^{-1} cm^{-3} [33]. Further details on the kinetic measurements are given elsewhere [34].

2.4. Infrared investigations

In situ IR investigations were performed in a DRIFTS configuration with a Nicolet Magna 560 spectrometer, equipped with a liquid N_2-cooled MCT narrow-band detector and a commercial in situ reaction cell unit from Harricks (HV-DR2). This setup allows measurement in a continuous gas flow and at elevated temperatures. The reaction mixture was similar to that used in the activity measurements. Typically, 400 scans (acquisition time 3 min, nominal resolution 8 cm^{-1}) were co-added for one spectrum. The infrared data were evaluated in Kubelka–Munk units, which are linearly related to the adsorbate concentration [35] (for deviations from a linear relation, see Ref. [36]). The background spectra were measured in pure N_2. A gas chromatograph (Chrompack CP 9001) connected to the exhaust of the DRIFTS cell was used to analyze the product gas stream; for further details, see Ref. [37].

3. Results

3.1. Catalyst surface characterization (TEM, XPS)

Based on ICP-AES measurements, ~85% of the initial Au content was removed by the leaching procedure, resulting in Au loadings of 0.4 and 0.5 wt% on the Au/CeO_2 catalysts with 188 and 78 m^2 g^{-1}, respectively (2.8 and 2.7 wt% Au before leaching).

The presence of Au nanoparticles before and after leaching, along with the Au particle size distribution on the non-leached catalysts, were tested and determined by TEM. After reductive pretreatment at 200 °C, the non-leached catalysts exhibited a homogeneous distribution of Au nanoparticles with a mean diameter of about 2 nm (supplementary information, Fig. S1a), in agreement with earlier findings [5,15,24]. After leaching, we found no Au nanoparticles independent of the subsequent treatment [vacuum drying (*L025*) or calcination at 400 °C (*LC400*)] (see supplementary information, Fig. S1b). Thus, the Au nanoparticles were completely removed during the leaching step, in agreement with findings of other groups [6,8–10,38]. A small Au (111) signal in the XRD measurements on the *LC400* sample indicates that some Au^0 particles were formed during calcination (~2 nm diameter based on the XRD measurements). This is also supported by a small Au^0 contribution in the Au(4f) peak.

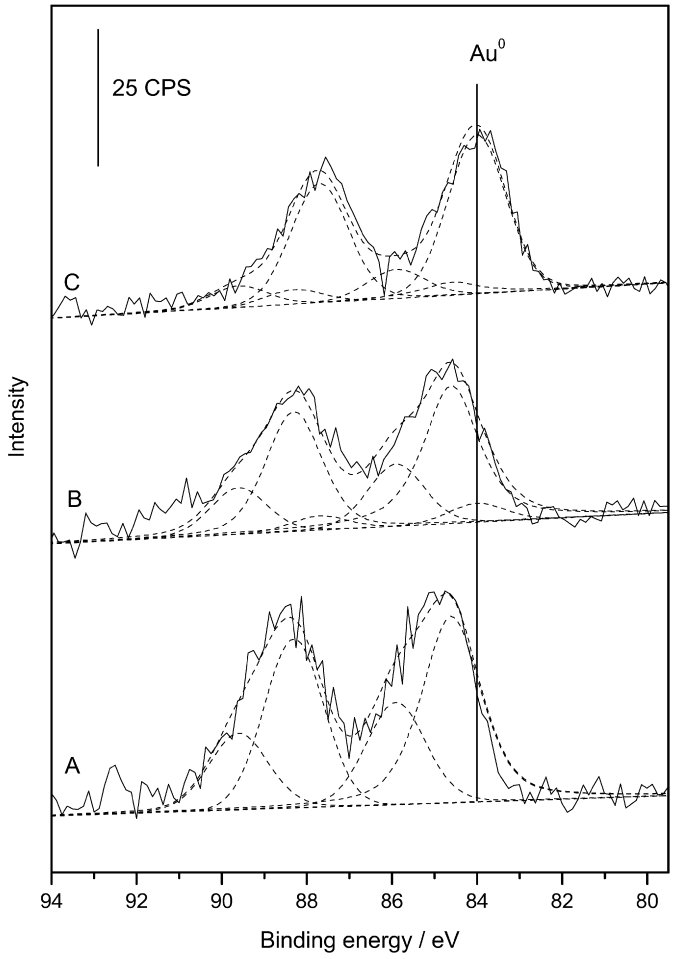

Fig. 1. XP spectra of the Au(4f) region recorded on (A) the leached + vacuum dried *L025* Au/CeO_2 catalyst and (B) on the leached + calcined *LC400* catalyst (0.4 wt% Au, 188 m^2 g^{-1}). (C): (B) + 1000 min WGS reaction in dilute water gas (1 kPa CO, 2 kPa H_2O in N_2) at 180 °C.

XP survey spectra of the Au/CeO_2 catalyst recorded after leaching and vacuum drying (Fig. S2) do not show any additional signals compared to the original catalyst. In particular, no new signals related to nitrogen or carbon containing species can be resolved. Based on these results and the DRIFTS background spectra (not shown), surface poising of the leached catalyst by adsorption of CN^- or other nitrogen-containing species remaining from the leaching procedure can be ruled out.

The oxidation state of the Au species gold remaining after leaching was determined from higher-resolution scans of the Au(4f) region (Fig. 1). For quantitative evaluation, we used a formal description by three different Au states, with Au(4f) BEs of 84.0, 84.6, and 85.9 eV, respectively [6,8,39,40]. The first and last peaks can be attributed to (bulk) metallic Au^0 and Au^{3+} (Au_2O_3) species [39–42]. A peak at 84.6 eV was assigned to Au^+ species (difference between Au^0 and Au^+ of 0.6 eV) [6,8,9]. This is also supported by results on gold–organic compounds, where, depending on the respective ligands, BEs of 84.6–85.9 eV were obtained for Au^+ species [43–46]. On the other hand, BE shifts of 0.5–0.9 eV relative to the bulk Au^0

Table 1
Fraction of different Au states in the total amount of Au in the non-leached and leached catalysts after different treatments as indicated and after subsequent water gas shift reaction

Catalyst treatment	*L025*	*L025* + 1000 min	*LC400*	*LC400* + 60 min	*LC400* + 1000 min	Non-leached	Non-leached-*H200*
Au amount (wt%)	0.4		0.4		0.4	2.8	2.8
Au^{3+} (%)	33	15	25	9	14	19	19
$Au^{0'}$ (%)	67	42	68	9	9	58	26
Au^{0} (%)	0	43	7	82	77	23	55
$I_{Au(4f)}/I_{Ce(3d)}$	0.01	0.01	0.01	0.01	0.01	0.21	0.05

value were obtained as final state effects in small Au clusters [47,48]. Thus this peak can be equally attributed to a final state-shifted Au^0 state at BEs $\geqslant$ 84.0 eV [49]. This indeed is favored by us, as discussed in more detail below. In what follows, this state is denoted as a $Au^{0'}$ state, but it should be kept in mind that the BE of the related Au(4f) peak was found to be similar to that of the Au^+ state in previous work [6,8,9].

XP spectra were recorded after leaching and drying overnight in vacuum (*L025*) (Fig. 1A), after subsequent calcination at 400 °C (*LC400*) in air (Fig. 1B), and after reaction of the *L025* (not shown) and *LC400* catalysts for 1000 min in dilute water gas (1 kPa CO, 2 kPa H_2O in N_2) (Fig. 1C). The main XPS results are listed in Table 1. For comparison, we also include the respective values obtained on a comparable non-leached Au/CeO_2 catalyst (*H200* conditioning) [15]. As expected from the ICP-AES data, the $I_{Au(4f)}/I_{Ce(3d)}$ ratio decreased to about 20% relative to the non-leached catalyst (Table 1). This decrease in Au content agrees well with the Au^{3+} content of 19% on the non-leached catalyst (Table 1), supporting the assumption that only these ionic species are not removed by the leaching process.

Using the above fitting procedure, we found no metallic Au signal on the leached and dried *L025* Au/CeO_2 samples, in close agreement with previously published data [6,8,9,38]. After calcination at 400 °C, the Au(4f) signal extended to lower BEs, and ∼7% metallic Au (of the residual Au amount) was found. The formation of metallic Au^0 can be explained by thermal decomposition of cationic gold species under these conditions [13,47,50,51]. After 1000 min of WGS reaction on the leached and calcined *LC400* catalyst, about 75% of the Au species exhibited metallic character, and the amount of $Au^{0'}$ and Au^{3+} species was reduced accordingly. Spectra recorded after 60 min of reaction showed a similar composition as those obtained after 1000 min of reaction, demonstrating that the reaction-induced reduction of the catalyst is rather fast and fully completed after 1 h. Similar measurements performed on the vacuum-dried and leached *L025* catalyst, showed a significantly lower metallic Au^0 content after 1000 min reaction. The much slower reduction kinetics can be explained most simply by an autocatalytic reduction process, with metallic Au^0 species acting as catalyst for further reduction. The strong change in the Au oxidation state correlates well with our earlier results of a pronounced reduction of the "Au^{n+}" species on non-leached Au/CeO_2 catalysts during the WGS reaction [24].

As mentioned above, the pronounced up-shift of the Au(4f) peak after leaching can be explained not only by a cationic Au species, but also by a particle size-induced final state effect [48,49,52]. Such effects were responsible for an 0.6–0.9 eV up-shift of the Au(4f) peak relative to bulk metallic Au on non-conditioned Au/TiO_2 catalysts [51,53], and similar shifts also were reported for small Au clusters deposited on diamond or SiO_2 substrate [48,54]. With increasing particle size, the Au(4f) peak would shift back to the metallic Au^0 position. This is exactly the behavior that would be expected for the present case, with very small Au^0 aggregates after leaching and increasing Au particle sizes on calcination or (even more pronounced) long-term reduction during reaction. In fact, the very small Au particles noted in the combined TEM and ICP-AES results necessarily require a final state shift of the Au(4f) peaks on the leached catalysts. As a result, we favor an interpretation of the broad, low BE Au(4f) peak at 84.0–84.6 eV, which was related to very small, possibly slightly charged Au particles rather than to a mixture of larger, metallic Au^0 nanoparticles and cationic Au^+ species. With increasing Au particle size, a mixture of different particle sizes led to a superposition of peaks at different positions, and the entire peak broadened and shifted to lower BE. (It also should be noted that charging effects related to a charge transfer from the ceria surface to the Au particle would decrease with Au particle size, similar to the final state effect.) The resulting peak broadening agrees well with the observation for the *L025* and *LC400* samples. This interpretation appears to be a physically more plausible explanation for the low BE Au(4f) intensity at 84.0–84.6 eV than the formal description by two peaks. However, the latter explanation does have the advantage of providing a semiquantitative measure of the growth of very small Au particles. Therefore, we still used the three-peak fitting procedure to describe the Au(4f) signal. Consequences of this reassignment of the $Au^{0'}$ peak at 84.6 eV on the reaction mechanism are discussed below.

3.2. Activity and stability of the Au/CeO_2 catalysts after different conditioning procedures

The evolution of the WGS reaction rates on Au/CeO_2 (188 $m^2\,g^{-1}$) during the reaction in dilute water gas on the before (2.8 wt% Au) and after leaching (0.4 wt% Au) is illustrated in Fig. 2. The resulting activities are collected in Table 2. Comparing the rates after 1000 min of reaction shows that the catalyst mass normalized activity was significantly lower (by ∼2 orders of magnitude) after leaching (*L025*) than before leaching, using the *H200* pretreated non-leached Au/CeO_2 catalyst as a reference (*H200*: 2.0×10^{-5} mol $g_{cat}^{-1}\,s^{-1}$, *L025*: 2.0×10^{-7} mol $g_{cat}^{-1}\,s^{-1}$). Using the Au mass-normalized activity, the differences in activity were significantly smaller (*H200*:

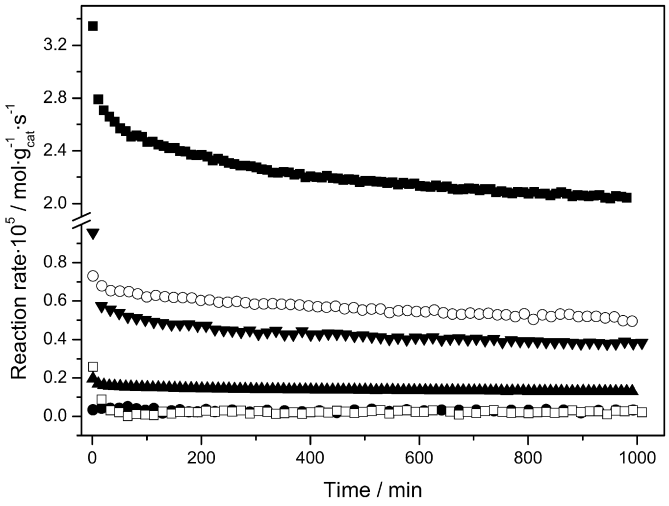

Fig. 2. Activity of the Au/CeO_2 catalysts in dilute water gas (1 kPa CO, 2 kPa H_2O in N_2) at 180 °C. (■) Non-leached Au/CeO_2 (2.8 wt% Au, *H200*), (□) leached + vacuum dried *L025* Au/CeO_2 (0.4 wt% Au), (○) leached + calcined *LC400* Au/CeO_2 (0.4 wt% Au), (▼) leached + calcined + H_2 treated *LC400/H200* Au/CeO_2 (188 $m^2\,g^{-1}$), (●) leached + vacuum dried + H_2 treated *L025/H200* Au/CeO_2 (188 $m^2\,g^{-1}$), (▲) non-leached Au/CeO_2 (141 $m^2\,g^{-1}$, 0.2 wt% Au, *H200*).

Table 2
Catalytic activity of Au/CeO_2 catalysts for the WGS reaction after different pre-/post-treatment procedures

Au/CeO_2 catalyst	Reaction rate (mol $g_{Au}^{-1}\,s^{-1}$)	Reaction rate (mol $g_{cat}^{-1}\,s^{-1}$)
Non-leached *H200*	7.2×10^{-4}	2.0×10^{-5}
L025	5.1×10^{-4}	2.0×10^{-7}
L025/H200	7.5×10^{-4}	3.0×10^{-7}
LC400	1.3×10^{-3}	5.0×10^{-6}
LC400/H200	9.8×10^{-4}	3.8×10^{-6}

7.2×10^{-4} mol $g_{Au}^{-1}\,s^{-1}$, *L025*: 5.1×10^{-5} mol $g_{Au}^{-1}\,s^{-1}$). The activity of the leached catalysts depended significantly on the catalyst treatment after leaching, as evidenced by the much higher activity of the leached and calcined *LC400* catalyst (curve ○, 5×10^{-6} mol $g_{cat}^{-1}\,s^{-1}$). Further processing of the *L025*/*LC400* catalysts at 200 °C in H_2 (*H200*), in contrast, had little effect on the WGS activities. The resulting activities (*L025/H200*, curve ●, 3×10^{-7} mol $g_{cat}^{-1}\,s^{-1}$; *LC400/H200*, curve ▼, 3.8×10^{-6} mol $g_{cat}^{-1}\,s^{-1}$) differed little from those of the respective leached catalysts before additional *H200* treatment. Because the treatment after leaching did not affect the Au loading, the trends described for the catalyst mass-normalized activities are also valid for the Au mass-normalized activity. For comparison with non-leached catalysts, the loss of Au during leaching must be considered. This leads to an increase in the Au mass-normalized activity by a factor of ∼2 for the leached and calcined catalysts (*LC400*, 1.3×10^{-3} mol $g_{Au}^{-1}\,s^{-1}$) compared with the standard non-leached *H200* catalyst (7.2×10^{-4} mol $g_{Au}^{-1}\,s^{-1}$).

These results agree completely with data of Kim and Thompson [10], who found a decrease in the catalyst mass normalized activity to about 1/16 of the original value after leaching and subsequent reductive treatment (4% H_2/N_2, 200 °C). The Au mass-related activity decreased to about 40% of the initial value. In contrast, these results differ distinctly from the previous findings of the group of Flytzani-Stephanopoulos [6,8,9], who found no change in the catalyst mass-normalized reaction rates (depending on the catalyst 1–3 × 10^{-6} mol $g_{cat}^{-1}\,s^{-1}$ in 1 kPa CO, 2 kPa H_2O in N_2, 175 °C [2]) after removal of the Au nanoparticles (remaining Au content ∼10% of the initial value). Possible explanations for the discrepancy between the results of Flytzani-Stephanopoulos and coworkers and those of Kim and Thompson and the present study may be linked to the presence of additional 10% La or Gd in the ceria support or, more likely, the very different activities of the non-leached catalysts used for comparison [6,8,9,38].

The activity of the non-leached *H200*-conditioned Au/CeO_2 catalysts used as a standard in the present study was about 10 times higher than that of the catalyst used by Fu et al. [2]. Among other reasons, this may be related to the very different mean Au particle sizes of ∼2 nm in the present study [5,15,24], whereas for the Au/CeO_2 catalysts used by the Flytzani-Stephanopoulos group, the Au particle size was around 5 nm (in some cases up to 36 nm) [2,6,8,55]. After leaching this calcined catalyst (Au removal ∼90%), the catalyst was calcined in air at 400 °C. This procedure was identical to that used for the *LC400* catalyst, and should result in a very active catalyst. Therefore, the small change in reaction rate observed by Fu et al. on leaching can be tentatively explained by a combination of low activity of the non-leached catalyst and high activity of the resulting leached and calcined catalyst. In contrast, in the leaching experiments reported by Kim and Thompson, the activity of the non-leached catalyst used for comparison is very high (18×10^{-6} mol $s^{-1}\,g_{cat}^{-1}$), and, accordingly, the loss of activity on leaching is much more pronounced. (Note that the WGS activity measurements were performed in realistic reformate in the work by Kim and Thompson [8,10], whereas the present kinetic data and those of Fu et al. [2,6] were measured in idealized and realistic reformate.)

Based on the absence of Au nanoparticles in their TEM and XRD measurements, Fu et al. concluded that on the leached catalyst, Au is present as cationic $Au^{\delta+}$ species only. Consequently, this was identified as an active species for the WGS reaction [6]. Kim and Thompson, on the other hand, came to the opposite conclusions, suggesting nanocrystalline Au particles as active species [10]. Our activity data seem to support their point of view in so far as removal of the Au nanoparticles resulted in a pronounced loss of activity; that is, the Au nanoparticles contributed significantly to the overall WGS activity under our reaction conditions.

Further information on the reaction behavior over the leached catalysts was obtained by comparison with the reaction behavior of non-leached Au/CeO_2 catalysts of similar Au loadings, comparison of the deactivation behavior of leached and non-leached catalysts, and the activation energies determined for the different catalysts. First, we compared the activity of the catalyst after leaching and calcination (*LC400*, 0.4 wt% Au) with that of a non-leached Au/CeO_2 catalyst with a similarly low Au loading (0.2 wt% Au, 141 $m^2\,g^{-1}$, conditioned by H_2

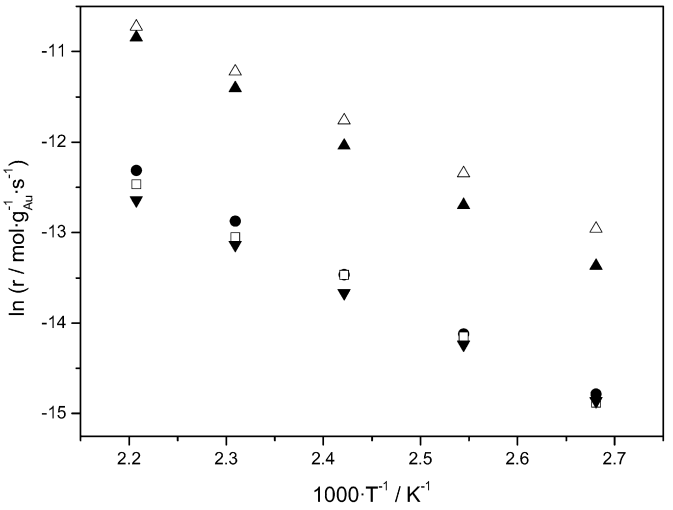

Fig. 3. Arrhenius plot of the temperature-dependent WGS reaction rates (mol g_{Au}^{-1} s^{-1}) over non-leached, *H200* pretreated Au/CeO_2 catalysts ((△) 78 m^2 g^{-1}, 2.7 wt% and (▲) 188 m^2 g^{-1}, 2.8 wt% Au), over leached + calcined Au/CeO_2 catalysts ((●) *LC400/N200*, 188 m^2 g^{-1}, 0.4 wt% Au; (□) *LC400/H200*, 188 m^2 g^{-1}, 0.4 wt% Au; (▼) *LC400/N200* 78 m^2 g^{-1}, 0.5 wt% Au). The rates were measured after 1000 min reaction to reach steady-state conditions and at least 60 min equilibration time per data point.

treatment, *H200*, Fig. 2, curve ▲). The Au content of the latter catalyst was about half, and the activity was only 1/4 to 1/3, of that of the *LC400* Au/CeO_2 catalyst. These findings agree rather well with the above finding that the Au mass-normalized activity after leaching and calcination was about double of that of the non-leached, *H200* treated catalyst. Therefore, the high Au mass-normalized activity of the leached catalyst was not exceptionally high, but was in the range of activities obtained for catalysts with comparable Au loadings [5].

The deactivation behavior of the non-leached and leached catalysts (see Fig. 2) was largely similar, with about 26% deactivation over 1000 min in idealized reformate [5,14,15,24]. Therefore, there is little difference between leached and non-leached catalysts in this respect as well.

Finally, the apparent activation energy for the reaction in dilute water gas was determined on two different Au/CeO_2 catalysts with 78 and 188 m^2 g^{-1} BET surface area for both the non-leached catalysts and after leaching and calcination. The measurements were performed in the temperature range of 100–180 °C. Before the activity measurements, the leached catalysts were pretreated in H_2 (*LC400/H200*) or in inert atmosphere (*LC400/N200*) at 200 °C, and then exposed for 1000 min to the reaction atmosphere to reach quasi-steady-state conditions and exclude further deactivation during the temperature-dependent measurements. For each temperature, the reaction rate was followed for at least 1 h. The results are summarized in Fig. 3 and Table 3. We found virtually no differences in the apparent activation energies before and after leaching, with activation energies of 42–45 kJ mol^{-1} on the Au/CeO_2 catalyst with 188 m^2 g^{-1} surface area and slightly lower values on the sample with 78 m^2 g^{-1} (39 kJ mol^{-1}). These results agree well with the results of previous leaching studies, which also showed no change in the activation energy on leaching [6,8–10]. This

Table 3
Apparent activation energy of the WGS reaction in dilute water gas on leached + calcined Au/CeO_2 catalysts after different post-treatments (1 kPa CO, 2 kPa H_2O in N_2)

Surface area (m^2 g^{-1})	188[a]	188[a]	188[a]	78[b]	78[b]
Leaching	−	+	+	−	+
Au amount (wt%)	2.8	0.4	0.4	2.7	0.4
Calcination	−	+	+	−	+
Pre-treatment (after calcination)	*H200*	*LC400/H200*	*LC400/N200*	*H200*	*LC400/N200*
E_{act} (kJ mol^{-1})	44.5	41.7	43.5	38.9	39.0

was considered evidence of a similar reaction mechanism in both cases. The data also agree with our earlier findings of an increasing activation energy with increasing BET surface area [15] and a constant activation energy of 40 ± 2 kJ mol^{-1} for Au/CeO_2 catalysts with 0.8–12.6 wt% Au at a constant surface area (188 m^2 g^{-1}) [5].

In total, the kinetic measurements lead to the following conclusion on the nature of the active site/species: If only cationic gold species would act as active centers in the WGS reaction, as proposed previously [6,8,9,38], we would expect a much more pronounced decay of the reaction rate during the activity measurement on the leached catalysts than on the non-leached catalyst. In this measurement, the "normal" deactivation observed on non-leached Au/CeO_2 catalysts under similar reaction conditions [5,14,24], would be enhanced on the leached catalyst due to the reaction-induced formation of metallic Au nanoparticles (see Section 3.1). Such an effect was not observed, however. Instead, we found similar deactivation behavior for both the non-leached and leached and calcined catalysts. On the other hand, if only metallic Au^0 nanoparticles were the active center, as proposed previously [10–12], then the activity of Au/CeO_2 catalysts should decrease less or even increase during reaction, because the "normal" deactivation is counteracted by the reaction-induced increase in metallic Au^0 nanoparticles. This was not observed (see above). Although other reaction models are also conceivable, the simplest explanation for the combined observations is a reaction mechanism in which both ionic Au species and Au^0 nanoparticles contribute to the reactivity.

3.3. Surface composition (DRIFTS)

The influence of removing the Au nanoparticles on the adsorption of reactants and on the production of adsorbed byproducts during the WGS reaction in dilute water gas was investigated by in situ DRIFTS measurements. In these measurements, we followed the reaction over 1000 min on leached Au/CeO_2 catalysts (188 m^2 g^{-1} BET surface area) after drying in vacuum (*LC025*) and after subsequent calcination in air at 400 °C (*LC400*) (Figs. 4c, 4d and 5). For comparison, similar measurements were performed on pure ceria (188 m^2 g^{-1}) under identical reaction conditions (Figs. 4a and 4b).

For the pure ceria support, three main peaks at 1588, 1369, and 1292–1302 cm^{-1} were observed in the frequency range of the OCO-bending vibrations (Fig. 4a). The first peak is assigned to bidentate formate [20,56,57]; the other two peaks are related

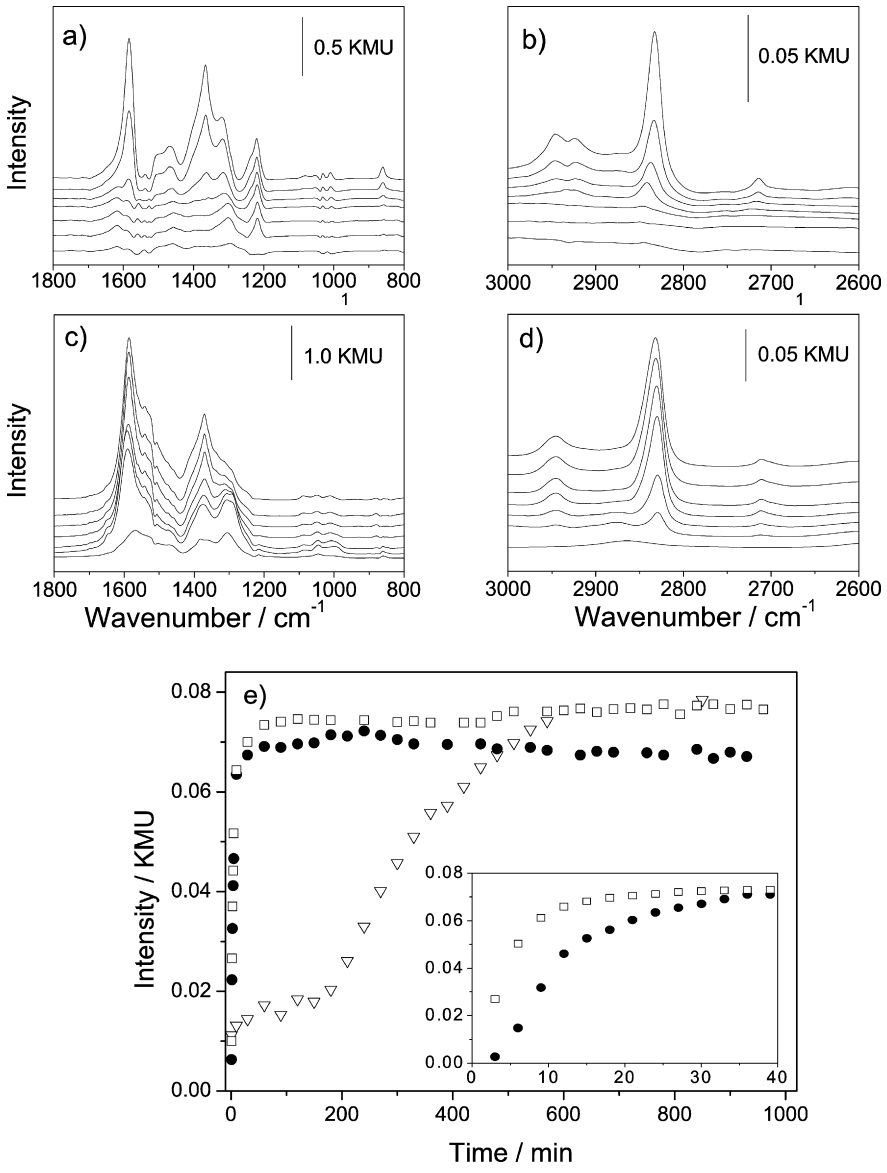

Fig. 4. Series of DRIFT spectra obtained during the WGS reaction in dilute water gas (1 kPa CO, 2 kPa H_2O in N_2) over 1000 min on pure ceria (a, b) and on the leached + dried Au/CeO_2 *L025* catalyst (c, d). (a) Detail spectra of the OCO region, (b) detail spectra of the C–H region on pure ceria (from bottom to top after 34 s, 10 min, 30 min, 150 min, 210 min, 390 min, 850 min). (c) Detail spectra of the OCO region, (d) detail spectra of the C–H region on the leached + dried Au/CeO_2 *L025* catalyst (from bottom to top after 23 s, 1 min, 4 min, 10 min, 30 min, 240 min, 1000 min). (e) Temporal evolution of the bidentate formate intensity (peak at 2831 cm^{-1}) on pure ceria (▽) and on the leached Au/CeO_2 catalysts, *L025* (□) and *LC400* (●) (data Fig. 5) upon reaction in dilute water gas. Inset: fast DRIFTS measurement of the initial formate formation (catalysts/conditions as in main figure). Full spectra are available as supplementary material, Fig. S3.

to carbonate species (see [14,15] and references therein). In the C–H region (Fig. 4b), the peaks at 2831 and 2944 cm^{-1} are related to bidentate and bridged formate species, respectively [56,58–60]. During the first 30-min reaction, mainly carbonate species and molecularly adsorbed water (1618 cm^{-1}) [20,61,62] are built up. In addition, the intensity of the bidentate and bridged formate-related signals grows slowly (Fig. 4b). The low formate formation rate can be related to the slow formation of OH_{ad} species on pure ceria compared with that on Me/CeO_2-supported catalysts (Me = Au, Pt, Ni, Co, Fe). The formation of OH groups by reaction of H_2O with ceria is known to be strongly enhanced by Ce^{3+} cations [15,20,21], which are formed much more easily on Au/CeO_2-supported catalysts than on pure ceria [4,13,18,19,22,63].

On the leached Au/CeO_2 catalysts, we find the same adsorbed (by)-products as on pure ceria, both after leaching and subsequent vacuum drying (*L025*; Figs. 4c and 4d) or after leaching and subsequent calcination (*LC400*; Fig. 5). In addition, the spectra resolve a feature at around 2126 cm^{-1} and an even weaker shoulder at around 2150 cm^{-1} related to adsorbed CO. Signals in these frequency ranges were previously related to CO_{ad} on $Au^{\delta+}$ (2123 cm^{-1}) [64–69] and on Au^{3+} species (2152 cm^{-1}) sites/species [64,68,70,71], and to a forbidden electronic transition on partly reduced ceria (2126 cm^{-1}) [13,29,57,72]. Considering the foregoing discussion of the XPS results, where we proposed the existence of very small, possibly slightly charged Au particles as origin of the up-shifted low BE Au(4f) state at 84.6 eV (see Section 3.1), it is important to note

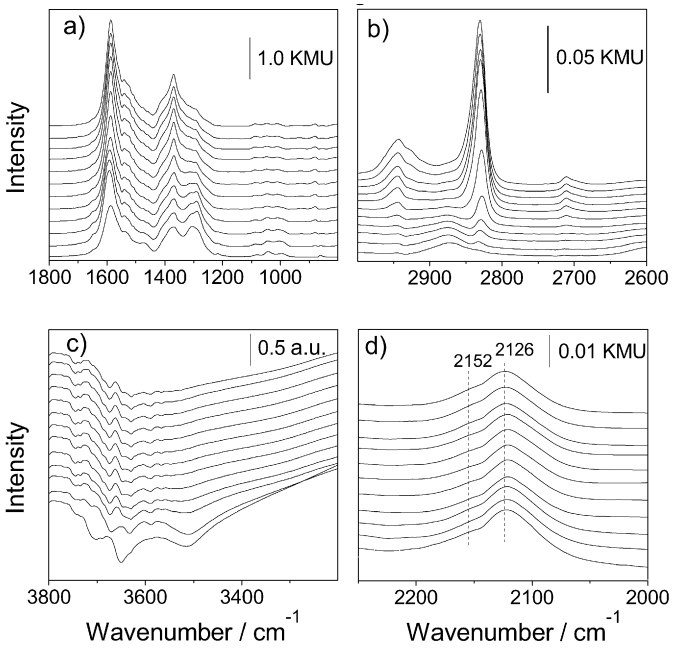

Fig. 5. Series of DRIFT spectra recorded during the WGS reaction in dilute water gas (1 kPa CO, 2 kPa H_2O in N_2) over 1000 min on a leached + calcined *LC400* Au/CeO_2 catalysts. (a) Detail spectra of the OCO-stretching vibration, (b) detail spectra of the C–H region, (c) detail spectra of the OH region (raw data), (d) detail spectra of the CO region (from bottom to top after 23 s, 35 s, 47 s, 1 min, 2 min, 4 min, 10 min, 30 min, 60 min, 240 min, 540 min, 1000 min).

that C–O stretch vibrations at similar and higher wavenumbers were previously reported for CO adsorbed on very small Au particles [73]. Based on these data, we assume that the observed peak at 2126 cm^{-1} contains contributions from the Ce^{3+}-related electronic transition and from CO adsorption on the small $Au^{0'}$ particles.

The most important difference between pure ceria and the Au-containing catalysts is the significantly higher formate formation rate on the leached Au/CeO_2 catalysts (both *L025* and *LC400*) compared with on the pure ceria support. This is illustrated by the much faster increase in the formate intensity with time on the leached catalysts shown in Fig. 4e. Bidentate formate species (peak at 2831 cm^{-1}), which were proposed as the dominant reaction intermediates under present reaction conditions [5], appeared already at the very beginning of the WGS reaction (within the first 30 s) on the leached and dried Au/CeO_2 catalyst (*L025*; Figs. 4c and 4d). Their intensity increased rapidly, leveled off after about 30 min, and reached a steady-state value after about 90 min the behavior on the leached and calcined catalyst (*LC400*) was very similar. But additional fast DRIFTS measurements (see Fig. 4e) revealed that the initial formate formation was significantly faster on *L025* than on *LC400*. In contrast, the final intensity of the formate signals under steady-state conditions was almost identical on all three samples. Because after leaching and drying, only cationic Au^{3+} and small Au clusters were present on the Au/CeO_2 catalyst (see above), and because bidentate formate formation occurs at a high rate during the initial phase of the reaction (Fig. 5), these species must be able to accelerate the formation of bidentate formates. A similarly rapid increase in the formate signals, along with a comparable steady-state intensity, were also observed on non-leached catalysts under these reaction conditions [15]. The comparable steady-state formate intensity obtained on the different samples (non-leached and leached catalysts, as well as pure ceria) indicates that the final formate coverage under these conditions was limited by the ceria surface, not by the amount or state of the Au.

Based on the XPS results, we would expect that during the reaction, the intensity of the signal for CO adsorbed on Au^0 nanoparticles, which is typically 2096–2100 cm^{-1} for Au/CeO_2 (1.5 kPa CO), increases considerably, paralleling the increasing intensity of the Au(4f) signal related to metallic Au nanoparticles. This is not the case, however. Whereas the peak centered at 2126 cm^{-1} was broad enough to include intensity at ~2100 cm^{-1}, the present data gave no indication of a change with time during the reaction. Both the total intensity and the shape of the CO_{ad} absorption peak remained virtually constant during the reaction. On the other hand, on the non-leached Au/CeO_2 catalyst, the CO_{ad} intensity decreased significantly during the reaction, in parallel with increasing carbonate intensity and decreasing CO_2 intensity and CO_2 formation rate. The constant CO_{ad} intensity is most simply explained by a compensation of two counteracting effects, deactivation (intensity decrease) and formation of Au^0 nanoparticles (intensity increase). Again, however, it should be noted that the peak at 2126 cm^{-1} is related to an electronic excitation (see above). Therefore, the remaining contribution from CO_{ad} adsorption may simply be too small to resolve reaction-induced changes.

Finally, in the spectral range typical for OH_{ad}-related bands (3200–3800 cm^{-1}), we found vibrational features at 3520, 3710, and 3655 cm^{-1} on both the leached and vacuum-dried *L025* (not shown) and the leached and calcined *LC400* catalysts. These features were attributed to linearly adsorbed (monodentate) and tridentate OH_{ad} groups on ceria ([13] and references therein). On exposure to the reaction gas mixture, the main changes in the OH_{ad}-related signals occurred during the first few minutes of the reaction. During that time, the above peaks disappeared, and new peaks appeared at 3590, 3630, 3675, and 3649 cm^{-1}. The latter peak is related to the "active" bridged OH_{ad} group [18,59,60]. Similar changes also were observed in our previous studies on non-leached catalysts [5,13–15]; thus, these data also provide no evidence for a change in the reaction mechanism due to partial removal of the nanocrystalline Au by leaching.

In a final experiment, we studied the influence of the Au nanoparticles on the decomposition of formate species, which we had proposed to represent the rate-limiting step for the WGS reaction on Au/CeO_2 catalysts under present reaction conditions [5]. We investigated this by following the decomposition of the accumulated bidentate formate species on the leached catalysts on changing from the reaction mixture (1 kPa CO, 2 kPa H_2O in N_2) to dilute water vapor (2 kPa H_2O in N_2) at 180 °C. Measurements were performed on both the leached and dried *L025* catalyst and the leached and calcined *LC400* catalyst. Sequences of IR spectra recorded during a 2 h reaction for reaching quasi-steady-state conditions and subsequent decomposition are shown in Fig. 6. During the first 15 min of

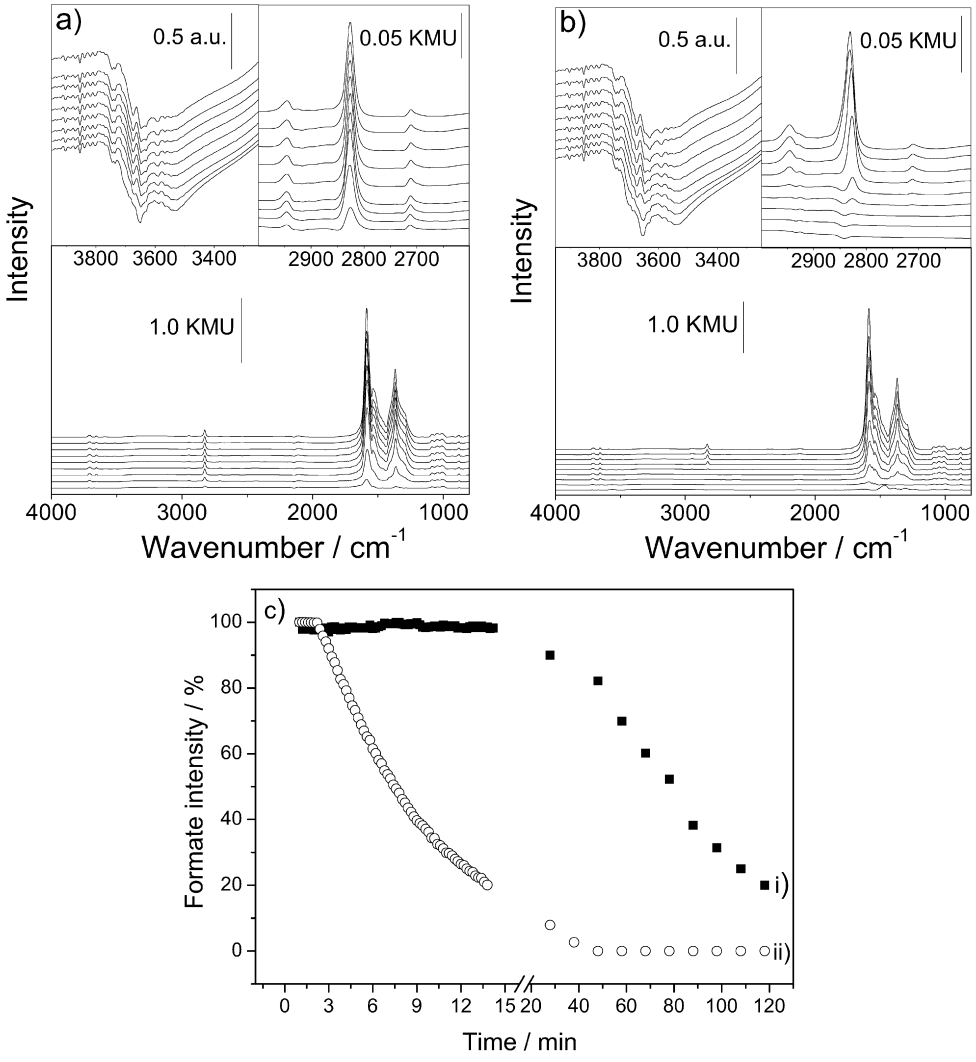

Fig. 6. Series of DRIFT spectra recorded during formate decomposition on reaction of formate pre-covered, leached Au/CeO_2 catalysts (after 120 min WGS reaction in dilute water gas) with 2 kPa H_2O/N_2: (a) on a *L025* catalyst and (b) on a *LC400* catalyst. Bottom: full spectrum, top right: detail spectra of the C–H region, top left: detail spectra of the OH region (raw data), from top to bottom after 0 s, 1 min, 2 min, 4 min, 10 min, 15 min, 30 min, 60 min, 120 min. (c) Formate decomposition on the (i) *L025* and the (ii) *LC400* leached Au/CeO_2 catalyst.

formate decomposition in water vapor, the bidentate formate intensity on the leached and dried Au/CeO_2 catalyst remained about constant (Figs. 6a and 6c). Over longer exposure times, the intensity decayed slowly, and after 2 h, the intensity of the bidentate formates decreased to about 20% of the initial value. In contrast, on the leached and calcined *LC400* catalyst, the bidentate formate intensity decayed rapidly (to 20% after $<$15 min) and completely disappeared after 30 min of reaction with water vapor (Figs. 6b and 6c). Thus, the decomposition of the reaction intermediate [5] was much faster on the leached and calcined *LC400* catalyst than on the leached and dried *L025* catalyst. Most simply, this difference is related to the higher content of metallic Au^0 species in the *LC400* catalyst compared with the *L025* catalyst after 120 min on stream when switching to 2 kPa water vapor. On the latter catalyst, the steady-state level of ~80% metallic Au^0 species was obtained already after 60 min (see Table 1), whereas on the latter catalyst, even after 1000 min, $<$50% of the Au content was converted into metallic Au^0 species. On a non-leached, *H200*-conditioned catalyst, the decomposition was again significantly faster (time for 50% decomposition, 80 s, compared with 300 s in the present case) [5], which is attributed to the much higher Au loading on that catalyst (2.6 wt%).

4. Discussion

The results presented above, in combination with previously reported results, lead to the following conclusions on the leaching process, on the nature of the Au species remaining after leaching and on the role of the different Au species in the WGS reaction:

1. Based on the good agreement between the initial amount of Au^{3+} species and the total amount of Au remaining after CN leaching, only the Au^{3+} species are stable against the leaching procedure. Both metallic Au^0 nanoparticles and the small $Au^{0'}$ aggregates associated with the Au(4f) signal at 84.0–84.6 eV (see item 2) were dissolved. This agrees well with the Au mass balance in the data of Fu et al. [6,8].

2. After leaching and post-treatment by drying in vacuum or by calcination in air, most of the (original) Au^{3+} was converted into a state characterized by Au(4f) intensity in the BE range 84.0–84.6 eV. We attribute this Au(4f) intensity to very small, possibly slightly charged Au^0 aggregates ($Au^{0'}$), with an Au(4f) signal slightly up-shifted compared with the BE of bulk Au (84.0 eV), due to particle size effects. The different sizes of the aggregates resulted in a sequence of up-shifted peaks in this energy range. The reassignment of the up-shift of the Au(4f) peaks to a particle size "final state" effect rather than to the formation of ionic Au^+ species (initial state effect) [6] fits well with recent observations on unconditioned Au/TiO_2 catalysts, where Au particles 1.3 nm and smaller resulted in similarly up-shifted Au(4f) signals [51,53].

3. The relative abundance of different Au species changed significantly during post-treatment after leaching and during the WGS reaction, with decreasing contents of Au^{3+} species and increasing content of Au^0 nanoparticles. These trends can be qualitatively explained by two different effects: thermal decomposition of Au oxide (Au^{3+} species) and thermally induced formation of very small $Au^{0'}$ aggregates and their growth into Au^0 nanoparticles. These steps, particularly the first one, are enhanced or hindered by the presence of a reductive (WGS reaction) or oxidative atmosphere (*LC400*). In none of these post-treatments was the Au^{3+} content found to increase again. The pronounced formation of Au^0 nanoparticles during the WGS reaction must be considered when interpreting the activity of the leached Au/CeO_2 catalysts and comparing it with XPS data taken before/without exposure to the reaction gas mixture.

4. Removal of the nanocrystalline Au^0 and of the very small $Au^{0'}$ aggregates led to a significant loss in (catalyst mass-normalized) WGS activity (to about 1%) when comparing a highly active non-leached catalyst (H_2 pretreated) with a similarly treated, leached *L025/H200* Au/CeO_2 catalyst. From these results, we conclude that metallic Au^0 nanoparticles and $Au^{0'}$ aggregates, with 55 and 26% abundance on the non-leached catalyst, respectively, played a significant role in the WGS reaction under the present reaction conditions rather than representing inactive spectator species. Therefore, "cationic gold species" cannot be identified as sole active species in the WGS reaction on Au/CeO_2 catalysts. Our findings and interpretation are in full agreement with the results of Kim and Thompson [10]. In contrast, Fu et al. found comparable (catalyst mass-normalized) reaction rates before and after leaching and thus proposed ionic Au species as the only active sites for the WGS shift reaction [6,8,9]. The different experimental observations can be explained at least partly by the rather low activity of the non-leached catalyst used as a reference by those authors (10% of the activity of the *H200*-conditioned catalyst used in this study). In contrast, the leached catalyst was calcined subsequently, and thus was in a very active state (comparable to that of the leached and calcined *LC400* catalyst). It should be noted that our data do not exclude the possibility that Au^{3+} species are active as well, but they are certainly not dominant for the activity.

5. The important role of nonionic Au species for the WGS activity is also emphasized by the strong effects induced by post-treatment of the leached Au/CeO_2 catalysts. Calcination of the leached catalyst (*LC400*) resulted in a much higher activity (by a factor of ∼25) than that obtained for a vacuum-dried (*L025*) catalyst with its much smaller content of Au^0 and $Au^{0'}$ species.

6. In contrast to the pronounced loss in catalyst mass-normalized activity on leaching, the decrease in Au mass normalized activity was much lower (*L025*: to ∼10%) or even increased by a factor of 2 for the *LC400* catalyst. On the other hand, the high Au mass-normalized activity of the leached and calcined catalyst was of similar magnitude as that of a non-leached and H_2-pretreated catalyst (*H200*) of comparable Au loading; they differed by a factor of 2. Therefore, the activity of the leached and calcined catalyst was high, but not exceptionally so. Accordingly, leaching did not result in a new, more active state of Au than would be accessible by conventional catalyst preparation.

7. Based on the much faster formate decomposition process on the *LC400* sample compared with that on the *L025* sample, we conclude that metallic Au^0 nanoparticles were more active for formate decomposition than Au^{3+} species and/or the very small $Au^{0'}$ aggregates. Here, it must be considered that in both cases, Au^0 particles were formed during the preceding WGS reaction (120 min), which was required for the build-up of formate species. However, this process was much more efficient on the *LC400* catalyst than on the *L025* catalyst. Formate formation, on the other hand, was strongly enhanced by Au species in general and was rapid from the very beginning. Because, based on the XPS measurements, there were no Au^0 nanoparticles on the *L025* sample at the beginning of the reaction, whereas formate formation was fastest on that sample, we conclude that Au^{3+} species and/or the very small $Au^{0'}$ particles associated with the Au(4f) peak at 84.0–84.6 eV were highly active for formate formation.

8. The comparable amount of formate species present under steady-state conditions on the vacuum-dried and the calcined leached catalyst, despite the very different (initial) formate decomposition activities, can be explained by two different schemes. Either it resulted from an inherently higher formate formation rate on the *LC400* catalyst, which can compensate for the higher decomposition rate on that catalyst, or, more plausibly, formate formation was limited by the similar formate storage capacity of the CeO_2 surface on both catalysts [15]. The latter explanation, which calls for a pronounced decay of the formate formation rate at coverages close to saturation, fits well with the observation that formate formation at lower coverages was much faster than formate decomposition at steady-state coverage on both *L025* and *LC400* under the present reaction conditions. (Under steady-state conditions, the rates for formate formation and decomposition must be identical.) It also is supported by the similar steady-state formate coverage obtained on the non-leached Au/CeO_2 catalyst.

9. The higher formate decomposition rate on the leached and calcined *LC400* catalyst with the much higher Au^0 content compared with the vacuum-dried *L025* catalyst, together with the much faster (initial) rate for formate formation than for formate decomposition, fit well with a mechanism for the WGS reaction that we had proposed earlier [5,14]. In that mecha-

nism, formate formation and decomposition represent the dominant reaction pathway under present reaction conditions, and, accordingly, we would expect higher WGS activity for a catalyst with a higher formate decomposition activity. It should be noted, however, that the dominant reaction pathway of the WGS reaction may vary with reaction conditions [1,24,29] and that other reaction pathways (e.g., through carbonate formation/decomposition) also have been proposed [1,29].

10. The similar deactivation behavior of leached and non-leached Au/CeO_2 catalysts, typically with a 26% loss of activity over 1000 min, points to a similar deactivation mechanism for both types of catalysts, which is not significantly affected by the nature of the Au species present on the catalyst and their abundance. For a mechanism in which Au^0 and $Au^{0'}$ particles/aggregates provide the active site, this would mean that these were equally affected. Furthermore, the similar correlation between decreasing reaction activity and increasing intensity of the monodentate carbonate-related signal (1415 cm^{-1}) with increasing reaction time on the leached and non-leached catalysts [14,15,24] indicates that these carbonate species were responsible for catalyst deactivation on the leached catalysts as well.

In summary, using the selective leaching process introduced by Fu et al. [6,8], these measurements can provide detailed information on the mechanism of the WGS reaction on Au/CeO_2 catalysts, on the nature and abundance of different Au species present on the leached and non-leached catalysts after different pretreatments and post-treatments, and on the role of the these different species in the reaction process. But the results are not as simple to interpret as perhaps was hoped after earlier experiments, because of the significant conversion of the Au species during catalyst treatments after the leaching process, such as drying, calcination, or even heating up to reaction temperature in inert gas, particularly during the WGS reaction itself. These processes make a simple mechanistic interpretation based on comparison of the catalytic activity before and after leaching impossible. Instead (and also for the seemingly simple leaching approach), extensive multitechnique measurements are required as the basis for mechanistic conclusions.

5. Conclusion

Using spectroscopic and structure-sensitive techniques for (in situ) catalyst characterization, we have shown that cyanide leaching of Au/CeO_2 catalysts, although selectively removing nonionic Au species, did not result in catalysts containing ionic Au^{3+} species only. Instead, post-treatment of the catalyst after leaching, such as drying or calcination, and in particular the WGS reaction itself, led to distinct changes in the nature and amount of Au species present on the catalyst—specifically, the formation of small $Au^{0'}$ aggregates and metallic Au^0 nanoparticles. The abundance of the different species depends strongly on the post-treatment of the leached catalyst, with higher temperatures and a reductive atmosphere favoring reduction of Au^{3+} species and formation of small $Au^{0'}$ aggregates and metallic Au^0 nanoparticles. Leaching led to a significant loss in catalyst mass-normalized activity, to 1% of the original activity when comparing catalysts treated in the same way after synthesis and after leaching, respectively. Therefore, Au^0 species, including both small aggregates and metallic nanoparticles, contribute significantly, if not predominately, to the WGS activity and cannot be considered (inert) spectator species. Based on in situ DRIFTS measurements, these species are particularly active for the decomposition of bidentate formate species.

Based on the very rapid formation of these formate species in the beginning of the WGS reaction, in combination with the comparable steady-state formate intensity and coverage on the leached and non-leached catalysts (for all post-treatments), we suggest that at coverages below saturation, formate coverage is determined mainly by formate decomposition, whereas formate formation is fast. Under steady-state conditions, both rates must be equal, which points to a pronounced decay of the formate formation rate at high coverages, close to saturation. This fits well with our previous proposal of bidentate formates acting as reaction intermediates in the dominant reaction pathway under these reaction conditions.

Acknowledgments

This work was supported by the Deutsche Forschungsgemeinschaft through Research Training Group (GRK) 328. The authors thank Dr. A. Chuvilin and L. Kroner for the electron microscopy and X-ray diffraction measurements.

Supplementary material

The online version of this article contains additional supplementary material.

Please visit DOI: 10.1016/j.jcat.2007.09.017.

References

[1] R. Burch, Phys. Chem. Chem. Phys. 8 (2006) 5483.
[2] Q. Fu, A. Weber, M. Flytzani-Stephanopoulos, Catal. Lett. 77 (2001) 87.
[3] T. Tabakova, F. Boccuzzi, M. Manzoli, J.W. Sobczak, V. Idakiev, D. Andreeva, Appl. Catal. B 49 (2004) 73.
[4] G. Jacobs, S. Ricote, P.M. Patterson, U.M. Graham, A. Dozier, S. Khalid, E. Rhodus, B.H. Davis, Appl. Catal. A 292 (2005) 229.
[5] R. Leppelt, B. Schumacher, V. Plzak, M. Kinne, R.J. Behm, J. Catal. 244 (2006) 137.
[6] Q. Fu, H. Saltsburg, M. Flytzani-Stephanopoulos, Science 301 (2003) 935.
[7] W. Deng, C. Carpenter, N. Yi, M. Flytzani-Stephanopoulos, Top. Catal. 44 (2007) 199.
[8] Q. Fu, W. Deng, H. Saltsburg, M. Flytzani-Stephanopoulos, Appl. Catal. B 56 (2005) 57.
[9] W. Deng, J. De Jesus, H. Saltsburg, M. Flytzani-Stephanopoulos, Appl. Catal. A 291 (2005) 126.
[10] C.H. Kim, L.T. Thompson, J. Catal. 244 (2006) 248.
[11] X. Wang, J.A. Rodriguez, J.C. Hanson, M. Perez, J. Evans, J. Chem. Phys. 123 (2005) 221101.
[12] D. Tibiletti, A.A. Fonseca, R. Burch, Y. Chen, J.M. Fischer, A. Goguet, C. Hardacre, P. Hu, D. Thompsett, J. Phys. Chem. B 109 (2005) 22553.
[13] A. Karpenko, Y. Denkwitz, V. Plzak, J. Cai, R. Leppelt, B. Schumacher, R.J. Behm, Catal. Lett. 116 (2007) 106.
[14] Y. Denkwitz, A. Karpenko, V. Plzak, R. Leppelt, B. Schumacher, R.J. Behm, J. Catal. 246 (2007) 74.
[15] A. Karpenko, R. Leppelt, V. Plzak, J. Cai, A. Chuvilin, B. Schumacher, U. Kaiser, R.J. Behm, Top. Catal. 44 (2007) 183.

[16] G. Jacobs, L. Williams, U. Graham, D. Sparks, B.H. Davis, J. Phys. Chem. B 107 (2003) 10398.
[17] G. Jacobs, L. Williams, U. Graham, G.A. Thomas, D.E. Sparks, B.H. Davis, Appl. Catal. 252 (2003) 107.
[18] G. Jacobs, P.M. Patterson, L. Williams, E. Chenu, D. Sparks, G. Thomas, B.H. Davis, Appl. Catal. A 262 (2004) 177.
[19] G. Jacobs, U.M. Graham, E. Chenu, P.M. Patterson, A. Dozier, B.H. Davis, J. Catal. 229 (2005) 499.
[20] T. Tabakova, F. Boccuzzi, M. Manzoli, D. Andreeva, Appl. Catal. A 252 (2003) 385.
[21] Lj. Kundakovic, D.R. Mullins, S.H. Overbury, Surf. Sci. 457 (2000) 51.
[22] A. Trovarelli, Catal. Rev. Sci. Eng. 38 (1996) 439.
[23] Catalysis by Ceria and Related Materials, Imperial College Press, London, 2002.
[24] A. Karpenko, R. Leppelt, J. Cai, V. Plzak, A. Chuvilin, U. Kaiser, R.J. Behm, J. Catal. 250 (2006) 139.
[25] A. Goguet, F.C. Meunier, D. Tibiletti, J.P. Breen, R. Burch, J. Phys. Chem. B 108 (2004) 20240.
[26] D. Tibiletti, A. Goguet, F.C. Meunier, J.P. Breen, R. Burch, Chem. Commun. (2004) 1636.
[27] D. Tibiletti, A. Goguet, D. Reid, F.C. Meunier, R. Burch, Catal. Today 113 (2006) 94.
[28] F.C. Meunier, D. Tibiletti, A. Goguet, D. Reid, R. Burch, Appl. Catal. A 289 (2005) 104.
[29] F. Meunier, D. Reid, A. Goguet, S. Shekhtman, C. Hardacre, R. Burch, W. Deng, M. Flytzani-Stephanopoulos, J. Catal. 247 (2007) 269.
[30] B. Schumacher, V. Plzak, M. Kinne, R.J. Behm, Catal. Lett. 89 (2003) 109.
[31] V. Plzak, J. Garche, R.J. Behm, Eur. Fuel Cell News 10 (2003) 16.
[32] M. Romeo, K. Bak, J. El Fallah, F. Le Normand, L. Hilaire, Surf. Interface Anal. 20 (1993) 508.
[33] P.B. Weisz, Chem. Eng. Prog. Symp. Ser. 55 (1992) 29.
[34] M.J. Kahlich, H.A. Gasteiger, R.J. Behm, J. Catal. 171 (1997) 93.
[35] I.M. Hamadeh, P.R. Griffiths, Appl. Spectrosc. 41 (1987) 682.
[36] J. Sirita, S. Phanichphant, F.C. Meunier, Anal. Chem. 79 (2007) 3912.
[37] M.M. Schubert, M.J. Kahlich, H.A. Gasteiger, R.J. Behm, J. Power Sources 84 (1999) 175.
[38] W. Deng, M. Flytzani-Stephanopoulos, Angew. Chem. 118 (2006) 2343.
[39] R. Holm, S. Storp, Appl. Phys. 9 (2003) 217.
[40] J.-J. Pireaux, M. Liehr, P.A. Thiry, J.P. Delrue, R. Caudano, Surf. Sci. 141 (1984) 221.
[41] D. Briggs, M.P. Seah, in: Practical Surface Analysis—Auger and X-Ray Photoelectron Spectroscopy, second ed., Wiley, Chichester, 1990.
[42] J.F. Moulder, W.F. Stickle, P.E. Sobol, K.D. Bomben, in: Handbook of X-Ray Photoelectron Spectroscopy, Perkin–Elmer, Eden Prairie, MN, 1992.
[43] H. Schmidbaur, J.R. Mandl, F.E. Wagner, D.F. Van de Vondel, G.P. Van der Kelen, J. Chem. Soc. Chem. Commun. 1976 (1976) 170.
[44] D.F. van de Vondel, G.P. van der Kelen, H. Schmidbaur, A. Wolleben, F.E. Wagner, Phys. Scr. 16 (1977) 364.
[45] P.M.Th.M. van Attekum, J.W.A. van der Velden, J.M. Trooster, Inorg. Chem. 19 (1980) 701.
[46] A. McNeillie, D.H. Brown, W.E. Smith, M. Gibson, L. Watson, J. Chem. Soc. Dalton 1980 (1980) 767.
[47] M. Haruta, S. Tsubota, T. Kobayashi, H. Kageyama, M.J. Genet, B. Delmon, J. Catal. 144 (1993) 175.
[48] H.-G. Boyen, A. Ethirajan, G. Kästle, F. Weigl, P. Ziemann, G. Schmid, M.G. Garnier, M. Büttner, P. Oelhafen, Phys. Rev. Lett. 94 (2005) 016804.
[49] G.K. Wertheim, S.B. DiCenzo, S.E. Youngquist, Phys. Rev. Lett. 51 (1983) 2310.
[50] G.J. Hutchings, M.S. Hall, A.F. Carley, P. Landon, B.E. Solsona, C.J. Kiely, A. Herzing, M. Makkee, J.A. Moulijn, A. Overweg, J.C. Fierro-Gonzalez, J. Guzman, B.C. Gates, J. Catal. 242 (2006) 71.
[51] E.A. Willneff, S. Braun, D. Rosenthal, H. Bluhm, M. Hävecker, E. Kleimenov, A. Knop-Gericke, R. Schlögl, S.L.M. Schroeder, J. Am. Chem. Soc. 128 (2006) 12052.
[52] S. Zafeiratos, S. Kennou, Surf. Sci. 443 (1999) 238.
[53] Y. Denkwitz, Z. Zhao, U. Hörmann, U. Kaiser, V. Plzak, R.J. Behm, J. Catal. 251 (2007) 363.
[54] H.-G. Boyen, T. Herzog, G. Kästle, F. Weigl, P. Ziemann, J.P. Spatz, M. Möller, R. Wahrenberg, M.G. Garnier, P. Oelhafen, Phys. Rev. B 65 (2002) 075412.
[55] Q. Fu, S. Kudriavtseva, H. Saltsburg, M. Flytzani-Stephanopoulos, Chem. Eng. J. 93 (2003) 41.
[56] C. Li, Y. Sakata, T. Arai, K. Domen, K. Maruya, T. Onishi, J. Chem. Soc. Faraday Trans. 85 (1989) 1451.
[57] E. Finocchio, M. Daturi, C. Binet, J.C. Lavalley, G. Blanchard, Catal. Today 52 (1999) 53.
[58] A.A. Davydov, in: Infrared Spectroscopy of Adsorbed Species on the Surface of Transition Metal Oxides, Wiley, Chichester, UK, 1984.
[59] T. Shido, Y. Iwasawa, J. Catal. 136 (1992) 493.
[60] T. Shido, Y. Iwasawa, J. Catal. 141 (1993) 71.
[61] A. Badri, C. Binet, J.C. Lavalley, J. Chem. Soc. Faraday Trans. 92 (1996) 4669.
[62] M.M. Natile, G. Boccaletti, A. Glisenti, Chem. Mater. 17 (2005) 6272.
[63] A. Badri, J. Lamotte, J.-C. Lavalley, A. Laachir, V. Perrichon, O. Touret, G.N. Sauvion, E. Quemere, Eur. J. Inorg. Chem. 28 (1991) 445.
[64] F. Boccuzzi, A. Chiorino, S. Tsubota, M. Haruta, J. Phys. Chem. 100 (1996) 3625.
[65] M. Manzoli, F. Boccuzzi, A. Chiorino, F. Vindigni, W. Deng, M. Flytzani-Stephanopoulos, J. Catal. 245 (2007) 308.
[66] F. Boccuzzi, A. Chiorino, J. Phys. Chem. B 104 (2000) 5414.
[67] F. Boccuzzi, A. Chiorini, M. Manzoli, P. Lu, T. Akita, S. Ichikawa, M. Haruta, J. Catal. 202 (2001) 256.
[68] J.C. Fierro-Gonzalez, B.G. Anderson, K. Ramesh, C.P. Vinod, J.W. Niemandsverdriet, B.C. Gates, Catal. Lett. 101 (2005) 265.
[69] M.A. Centeno, K. Hadjiivanov, Tz. Venkov, Hr. Klimev, J.A. Odriozola, J. Mol. Catal. A Chem. 252 (2007) 142.
[70] F. Boccuzzi, A. Chiorino, M. Manzoli, Surf. Sci. 454–456 (2000) 942.
[71] J. Guzman, S. Carrettin, A. Corma, J. Am. Chem. Soc. 127 (2005) 3286.
[72] F. Bozon-Verduraz, A. Bensalem, J. Chem. Soc. Faraday Trans. 90 (1994) 653.
[73] C. Lemire, R. Meyer, S.K. Shaikhutdinov, H.-J. Freund, Surf. Sci. 552 (2004) 27.